

# Random phase approximation-based local natural orbital coupled cluster theory

Ruiheng Song,<sup>1</sup> Xiliang Gong,<sup>1</sup> Aamy Bakry,<sup>1</sup> and Hong-Zhou Ye<sup>1,2, a)</sup>

<sup>1)</sup>*Department of Chemistry and Biochemistry, University of Maryland, College Park, Maryland, 20742*

<sup>2)</sup>*Institute for Physical Science and Technology, University of Maryland, College Park, Maryland, 20742*

(Dated: 5 January 2026)

Practical applications of fragment embedding and closely related local correlation methods critically depend on a judicious choice of a low-level theory to define the local embedding subspace and to capture long-range electrostatic and correlation effects outside the embedding region. Second-order Møller-Plesset perturbation theory (MP2) is by far the most widely used correlated low-level theory; however, its applicability becomes questionable in systems where MP2 is known to fail either quantitatively or qualitatively. In this work, we present the random phase approximation (RPA) as a promising alternative low-level theory to MP2 within the local natural orbital-based coupled-cluster (LNO-CC) framework. We demonstrate that RPA-based LNO-CC closely matches the performance of its MP2-based counterpart for systems with sizable energy gaps, while delivering significantly faster convergence toward the canonical coupled-cluster limit for metallic systems, particularly as the thermodynamic limit is approached. These results highlight the critical role of the low-level theory in fragment embedding and local correlation methods and identify RPA as a compelling alternative to the commonly used MP2.

## I. INTRODUCTION

Quantum embedding and fragment-based local correlation methods mitigate the steep computational cost of high-accuracy electronic structure theories such as coupled cluster<sup>1</sup> (CC) by applying these methods only to chemically meaningful local fragments.<sup>2–5</sup> Long-range electrostatic and correlation effects outside the fragments are instead treated with a low-level theory, rendering the overall approach computationally tractable. Representative examples include the use of one-body effective potentials in wavefunction-in-density functional theory embedding,<sup>4,6–9</sup> mean-field or correlated bath orbitals in density matrix embedding theory<sup>10–12</sup> (DMET) and its variants,<sup>13–18</sup> and correlated natural orbitals in the local natural orbital<sup>19–24</sup> (LNO) extension of cluster-in-molecule<sup>25–30</sup> (CIM) methods. In all such approaches, the choice of the low-level theory plays a pivotal role, as it controls the rate of convergence with fragment size and thus largely determines the practical efficiency of the method.

Second-order Møller-Plesset perturbation theory<sup>31</sup> (MP2) is by far the most widely used correlated low-level theory in quantum embedding and local correlation methods. MP2-based natural orbitals and long-range correlation corrections have a long history in local CC theories.<sup>32–37</sup> More recently, MP2-derived natural orbitals have also been adopted as correlated bath states in DMET<sup>15,38</sup> and dynamical mean-field theory<sup>39</sup> (DMFT), where they alleviate the disentanglement problems associated with mean-field baths<sup>40</sup> and enable an effective description of dynamical correlation in molecules and insulating solids. Despite these successes, the use of MP2 as a low-level theory becomes questionable in systems where MP2 is quantitatively inaccurate or even formally invalid. Two

prominent examples, which are the focus of the present work, are noncovalently bound molecules and molecular solids—where MP2 significantly overestimates intermolecular interaction energies<sup>41–44</sup>—and bulk metals, for which the MP2 correlation energy diverges in the thermodynamic limit<sup>45–47</sup> (TDL).

The random phase approximation<sup>48–50</sup> (RPA) provides a promising alternative to MP2 in both of these contexts.<sup>51–53</sup> By resumming the direct particle-hole ring diagrams to infinite order, RPA incorporates dynamical screening of the bare Coulomb interaction, leading to improved descriptions of noncovalent interactions<sup>54–61</sup> and metallic systems.<sup>62–70</sup> Within embedding frameworks, RPA has been most extensively explored in the form of constrained RPA (cRPA)<sup>71–74</sup> for Hamiltonian downfolding, where the RPA polarizability is used to construct effective screened interactions for a chosen active space. More recently, Schäfer and co-workers have demonstrated that RPA natural orbitals, obtained from first-order Green's functions,<sup>75</sup> can be used to accelerate embedding-based CC calculations.<sup>76,77</sup> Callahan and co-workers have demonstrated the use of RPA-based composite energy corrections to accelerate the convergence of CC calculations for uniform electron gas.<sup>78</sup>

In this work, we present an alternative route for incorporating RPA into fragment embedding and local correlation theories. Our approach is based on the direct ring coupled-cluster doubles (drCCD) formulation of RPA,<sup>79</sup> which provides direct access to RPA wavefunction amplitudes and can therefore be integrated seamlessly into existing MP2-based embedding and local correlation frameworks. We report an efficient implementation of RPA-based natural orbitals based on the factorized drCCD equation by Heßelmann<sup>80</sup> and Kállay<sup>81</sup> with asymptotic cost scaling more favorable than that of conventional MP2-based approaches. The effectiveness of RPA as a low-level theory is demonstrated within the LNO-CC framework, originally developed by Kállay and co-workers

<sup>a)</sup>Electronic mail: [hzye@umd.edu](mailto:hzye@umd.edu)

for molecules<sup>19–22</sup> and recently extended to both insulating and metallic solids by one of the authors.<sup>24,82,83</sup> Our numerical results for noncovalently bound molecules, molecular solids, and bulk metals indicate that RPA-derived LNOs are of comparable quality to their MP2-based counterparts, while composite energy corrections based on RPA and the closely related second-order screened exchange<sup>84</sup> (SOSEX) approximation lead to systematically faster convergence with respect to LNO truncation than MP2-based corrections. This improvement is particularly pronounced for metallic systems as the TDL is approached using increasingly dense  $k$ -point meshes. Together, these results highlight the critical role of the low-level theory in fragment embedding and local correlation methods and suggest RPA as a compelling alternative to the commonly used MP2.

The remainder of this paper is organized as follows. In section II, we briefly review the MP2-based LNO-CC formalism and introduce its RPA-based generalization, along with details of an efficient implementation for molecules and periodic solids. Computational details are given in section III. In section IV, we present benchmark results for two classes of systems where MP2 is known to be problematic: noncovalently bound molecular systems and bulk metals. Finally, section V summarizes our findings and outlines directions for future work.

## II. THEORY

Throughout the paper, we assume a spin-restricted Hartree-Fock (HF) reference wavefunction with  $N_{\text{occ}}$  occupied orbitals labelled by  $i, j, k, \dots$  and  $N_{\text{vir}}$  virtual orbitals labelled by  $a, b, c, \dots$ , which give rise to  $N_{\text{MO}}$  molecular orbitals labelled by  $p, q, r, \dots$ . The HF orbitals and their orbital energy are denoted by  $\psi_p$  and  $\varepsilon_p$ , respectively. The Hamiltonian in the HF orbital basis reads

$$\hat{H} = \sum_{\sigma} \sum_{pq} h_{pq} c_{p\sigma}^{\dagger} c_{q\sigma} + \frac{1}{2} \sum_{\sigma\sigma'} \sum_{pqrs} V_{pqrs} c_{p\sigma}^{\dagger} c_{r\sigma'}^{\dagger} c_{s\sigma'} c_{q\sigma} \quad (1)$$

where  $\sigma$  labels spin,  $h_{pq}$  and  $V_{pqrs}$  are the one- and two-electron integrals, with the latter in the (11|22) notation. The formula presented below apply directly to molecules and periodic solids with a single  $k$ -point sampling the first Brillouin zone. Extension to periodic calculations with a uniform  $k$ -mesh is straightforward following Ref 24 by first transforming the HF orbitals into the corresponding supercell representation with a single  $k$ -point.

### A. Local natural orbital-based coupled cluster (LNO-CC)

In conventional MP2-based LNO-CC, the HF occupied orbitals are first localized to obtain an equal number of localized orbitals (LOs),

$$\phi_I = \sum_i \psi_i U_{il}, \quad (2)$$

where the unitary matrix  $U$  is determined by maximizing a chosen orbital locality metric (e.g., Pipek-Mezey,<sup>85,86</sup> Foster-Boys,<sup>87</sup> and the maximally localized Wannier functions<sup>88</sup>). The LNOs associated with a given LO  $\phi_I$  are obtained from the eigenvectors of the MP2 one-particle density matrix constructed for  $\phi_I$ ,

$$\begin{aligned} \xi_k^{(I)} &= \sum_i \psi_i X_{ik}^{(I)}, \\ \xi_c^{(I)} &= \sum_a \psi_a X_{ac}^{(I)}, \end{aligned} \quad (3)$$

where the occupied-occupied and virtual-virtual blocks of the density matrix are given by

$$\begin{aligned} D_{ij}^{(I)} &= 2 \sum_{ab} t_{ialb}^{(1)*} \left( 2t_{jalb}^{(1)} - t_{jbIa}^{(1)} \right) = \sum_k n_k^{(I)} X_{ik}^{(I)} X_{jk}^{(I)*} \\ D_{ab}^{(I)} &= \sum_{jc} 2 \left( t_{Iajc}^{(1)} t_{Ibjc}^{(1)*} + t_{Icj}^{(1)} t_{Icj}^{(1)*} \right) \\ &\quad - \left( t_{Icj}^{(1)} t_{Ibjc}^{(1)*} + t_{Iajc}^{(1)} t_{Icj}^{(1)*} \right) = \sum_c n_c^{(I)} X_{ac}^{(I)} X_{bc}^{(I)*}. \end{aligned} \quad (4)$$

Here,  $t_{Iajb}^{(1)} = \sum_i U_{il} t_{iajb}^{(1)}$ , and

$$t_{iajb}^{(1)} = \frac{V_{iajb}^*}{\varepsilon_i + \varepsilon_j - \varepsilon_a - \varepsilon_b} \quad (5)$$

are the MP2 amplitudes and the asterisk symbol indicates complex conjugate. A commonly adopted approximation is to replace the full MP2 amplitudes in eq. (4) with their semi-canonical counterparts.<sup>19,24,32</sup> In this work, however, we employ the full MP2 amplitudes for LNO construction in order to maintain consistency with the RPA-based LNO construction discussed in section II B.

Because the orbital rotations in eq. (3) do not mix occupied and virtual subspaces, the resulting LNOs preserve the integer occupations of the underlying mean-field reference. Important occupied and virtual LNOs can therefore be selected independently to define a LO-specific local active space (LAS)  $\mathcal{A}^{(I)}$  that is optimized for capturing the correlation energy associated with  $\phi_I$ . In this work, active LNOs are selected by thresholding the eigenvalues of eq. (4), also known as LNO occupation numbers,

$$\begin{aligned} n_i^{(I)} &\geq \eta_{\text{occ}}, \\ n_a^{(I)} &\geq \eta_{\text{vir}}, \end{aligned} \quad (6)$$

where  $\eta_{\text{occ}}$  and  $\eta_{\text{vir}}$  are user-defined thresholds. Tightening these thresholds systematically enlarges the LAS by including additional LNOs.

The LNO-based LAS can be viewed as a correlated bath constructed for each individual LO, extending the mean-field bath concept employed in DMET<sup>10,11</sup> and related fragment embedding approaches.<sup>13</sup> If the initial LOs span both the occupied space and part of the virtual space—as is common in fragment embedding methods<sup>11,40</sup>—the LAS may be defined by combining a DMET-style mean-field bath derived from

Schmidt decomposition<sup>89</sup> with truncated LNOs obtained from the remaining orbital space.<sup>24</sup> This generalization enables the use of more flexible LO types, such as intrinsic atomic orbitals,<sup>10</sup> thereby facilitating the application of LNO-CC to systems with small energy gaps (e.g., metals), for which localization of the occupied orbitals alone can be numerically challenging.<sup>88,90</sup>

LNO-CC exploits the LNO-based LAS to approximate the canonical CC correlation energy. In this work, we focus primarily on LNO-CCSD and LNO-CCSD(T). The CCSD correlation energy is approximated as

$$E_{c,CCSD} \approx E_{c,LNO-CCSD} = \sum_I E_{c,LNO-CCSD}^{(I)} + \Delta E_{c,MP2}^{\text{ext}}, \quad (7)$$

where the first term collects CCSD correlation energies evaluated within the LAS of each LO, and the second term is an external correction that approximately accounts for correlation energy arising from orbitals outside the LAS at the MP2 level. To evaluate both contributions, a local Hamiltonian is constructed for each LO by projecting the full Hamiltonian  $\hat{H}$  onto the corresponding LAS,

$$\hat{H}^{(I)} = \sum_{\sigma} \sum_{pq \in \mathcal{A}^{(I)}} f_{pq}^{(I)} c_{p\sigma}^{\dagger} c_{q\sigma} + \frac{1}{2} \sum_{\sigma\sigma'} \sum_{pqrs \in \mathcal{A}^{(I)}} V_{pqrs} c_{p\sigma}^{\dagger} c_{r\sigma'}^{\dagger} c_{s\sigma'} c_{q\sigma}, \quad (8)$$

with  $f_{pq}^{(I)} = h_{pq} + \sum_{i \notin \mathcal{A}^{(I)}} (2V_{pqii} - V_{piiq})$ . Solving the CCSD equations for each  $\hat{H}^{(I)}$  yields the local CCSD amplitudes  $t_{ia}^{(I)}$  and  $t_{iajb}^{(I)}$  within the LAS. These amplitudes define the LO-resolved CCSD correlation energy,

$$E_{c,LNO-CCSD}^{(I)} = \sum_{jab \in \mathcal{A}^{(I)}} \tau_{iajb}^{(I)} (2V_{iajb} - V_{ibja}), \quad (9)$$

where  $\tau_{iajb}^{(I)} = t_{iajb}^{(I)} + t_{ia}^{(I)} t_{jb}^{(I)}$ . The MP2-based external correction is evaluated as the difference between the canonical MP2 correlation energy and its LNO-truncated counterpart,

$$\Delta E_{c,MP2}^{\text{ext}} = E_{c,MP2} - \sum_I E_{c,LNO-MP2}^{(I)}, \quad (10)$$

where

$$E_{c,LNO-MP2}^{(I)} = \sum_{jab \in \mathcal{A}^{(I)}} t_{iajb}^{(1)(I)} (2V_{iajb} - V_{ibja}). \quad (11)$$

The CCSD(T) correlation energy can be approximated in an analogous fashion; detailed expressions may be found in Ref 21 and 24.

Because each LAS consists of LNOs localized around a given LO, the MP2-based LNO-CC energy [eq. (7)] is accurate when the long-range component of the correlation energy is well described at the MP2 level. A key practical advantage of the LNO framework is its systematic improvability: tightening the truncation thresholds in eq. (6) enlarges the LAS and reduces the approximation error. In the limit of vanishing thresholds, the LAS spans the full orbital space, and LNO-CCSD and LNO-CCSD(T) recover their canonical counterparts. For fixed thresholds, the LAS size has been shown

to be asymptotically independent of system size, rendering LNO-CCSD and LNO-CCSD(T) linear-scaling methods.<sup>20,21</sup> In practice, however, the usefulness of the LNO approximation depends critically on the rate at which the error decays with LAS size, which is governed by the quality of the underlying low-level theory. In the following section, we introduce RPA as an alternative low-level theory for LNO-CC.

## B. RPA-based LNO-CC

As discussed in section II A, MP2 serves two distinct roles in conventional LNO-CC: (i) the construction of LNOs [eqs. (3) and (4)] and (ii) the evaluation of the external energy correction [eq. (10)]. The CC-based formulation of RPA<sup>61,79,91–94</sup> provides a natural alternative to MP2 for both tasks, leading to what we refer to as RPA-based LNO-CC. Within the CC framework, RPA is equivalent to the direct ring CCD (drCCD) approximation,<sup>79</sup> which retains only the direct particle-hole ring diagrams of CCSD. The RPA correlation energy is given by

$$E_{c,RPA} = E_{c,drCCD} = 2 \sum_{ijab} T_{iajb} V_{iajb}, \quad (12)$$

where the drCCD amplitudes  $T_{iajb}$  satisfy the nonlinear amplitude equation

$$B^* + \Delta \circ T + 2L^*T + 2TL + 4TBT = 0. \quad (13)$$

Here,  $B_{iajb} = V_{iajb}$ ,  $L_{iajb} = V_{iabj}$ , and  $\Delta_{iajb} = \epsilon_a + \epsilon_b - \epsilon_i - \epsilon_j$ . The symbol “ $\circ$ ” denotes the Hadamard (element-wise) product, and matrix multiplication is defined as  $(AB)_{iajb} = \sum_{kc} A_{iakc} B_{kcjb}$ . Because the nonlinear drCCD equations can admit multiple solutions,<sup>91,94,95</sup> we employ the level-shift preconditioner described in Ref 95 to ensure robust convergence to the physical solution.

The extension of LNO-CC from MP2 to RPA is straightforward thanks to the formal similarity between MP2 and drCCD amplitudes. Specifically, RPA-based LNOs are constructed from one-particle density matrices of the same form as eq. (4), but with the MP2 amplitudes [eq. (5)] replaced by the drCCD amplitudes  $T_{iajb}$ . The RPA-based external energy correction is defined analogously to eq. (10),

$$\Delta E_{c,RPA}^{\text{ext}} = E_{c,RPA} - \sum_I E_{c,LNO-RPA}^{(I)}, \quad (14)$$

where the LO-resolved RPA correlation energy follows directly from eq. (12),

$$E_{c,LNO-RPA}^{(I)} = 2 \sum_{jab \in \mathcal{A}^{(I)}} T_{iajb}^{(I)} V_{iajb}. \quad (15)$$

A well-known limitation of RPA is the neglect of exchange diagrams, which typically leads to an overestimation of the correlation energy due to self-interaction. Including exchange contributions in the evaluation of the drCCD correlation energy [eq. (12)] leads to the RPA+SOSEX method<sup>84</sup> (referred to as SOSEX for simplicity hereafter),

$$E_{c,SOSEX} = \sum_{ijab} T_{iajb} (2V_{iajb} - V_{ibja}), \quad (16)$$

which removes the one-electron self-interaction error inherent in RPA.<sup>80,84</sup> Employing SOSEX to evaluate the external energy correction leads to what we term the SOSEX-based LNO-CC approach,

$$\Delta E_{c,\text{SOSEX}}^{\text{ext}} = E_{c,\text{SOSEX}} - \sum_I E_{c,\text{LNO-SOSEX}}^{(I)}, \quad (17)$$

where the LO-resolved SOSEX correlation energy is given by

$$E_{c,\text{LNO-SOSEX}}^{(I)} = \sum_{jab \in \mathcal{A}^{(I)}} T_{Iajb}^{(I)} (2V_{Iajb} - V_{Ibjb}). \quad (18)$$

More generally, the RPA-based LNO-CC framework can be straightforwardly extended to incorporate other beyond-RPA correlation methods formulated within the CC framework,<sup>80,96</sup> which we leave for future work.

### C. Efficient implementation of RPA-based LNO-CC

The drCCD equation (13) can be solved efficiently using the quartic-scaling algorithms originally developed by Heßelmann<sup>80</sup> and Kállay.<sup>81</sup> In these approaches, the four-index amplitudes  $T_{Iajb}$  are factorized in terms of three-index intermediates,

$$T_{Iajb} = - \sum_w^{N_{\text{CD}}} \tau_{iaw} \left( \sum_P^{N_{\text{aux}}} U_{iaP} U_{jbP} \right) \tau_{jbw}, \quad (19)$$

where  $\tau_{iaw}$  are Cholesky factors of the orbital-energy denominator,<sup>97,98</sup>

$$(\Delta_{Iajb})^{-1} \approx \sum_w^{N_{\text{CD}}} \tau_{iaw} \tau_{jbw}, \quad (20)$$

and  $P$  labels the auxiliary basis functions used in density fitting (DF) of the electron repulsion integrals,<sup>99–101</sup>

$$\begin{aligned} B_{Iajb} &= \sum_P^{N_{\text{aux}}} J_{iaP} J_{jbP}, \\ L_{Iajb} &= \sum_P^{N_{\text{aux}}} J_{iaP} J_{jbP}^*. \end{aligned} \quad (21)$$

The three-index amplitudes  $U_{iaP}$  satisfy the factorized drCCD equation,<sup>80,81</sup>

$$U_{iaP} = J_{iaP}^* - \sum_w^{N_{\text{CD}}} \tau_{iaw} \left( \sum_Q^{N_{\text{aux}}} U_{iaQ} U_{jbQ} \right) J_{jbP}. \quad (22)$$

Equation (22) is independent of the four-index  $T$  amplitudes and therefore requires only  $O(N^3)$  memory, comparable to DF-MP2. The computational cost of solving eq. (22) scales as  $O(N^4)$ , which is asymptotically more favorable than DF-MP2.

Once the  $U$  amplitudes are obtained, the total RPA correlation energy can be evaluated without explicitly forming  $T$ ,

$$E_{c,\text{RPA}} = 2 \sum_{ia}^{N_{\text{aux}}} \sum_P^{N_{\text{aux}}} (J_{iaP}^* - U_{iaP}) J_{iaP}. \quad (23)$$

Similarly, the LO-resolved RPA correlation energy required for the external correction in eq. (14) can be evaluated using the local  $U$  amplitudes restricted to the LAS,

$$E_{c,\text{LNO-RPA}}^{(I)} = 2 \sum_{a \in \mathcal{A}^{(I)}} \sum_P^{N_{\text{aux}}} (J_{Iap}^* - U_{Iap}^{(I)}) J_{Iap}. \quad (24)$$

The evaluation of drCCD density matrices [eq. (4)] required for constructing RPA-based LNOs and the calculation of the SOSEX external correction [eq. (17)] both necessitate reconstructing the  $T$  amplitudes from the factorized representation in eq. (19). For each LO, the associated CPU and memory costs scale as  $O(N^4)$  and  $O(N^3)$ , respectively, with the peak memory requirement further reducible to  $O(N^2)$  by constructing  $T$  in batches.

The quartic-scaling drCCD algorithm was originally developed for molecular systems.<sup>80,81</sup> Here, we extend this framework to periodic solids with explicit  $k$ -point sampling, enabling periodic RPA-based LNO-CC calculations. The computational cost of the periodic drCCD implementation scales as  $O(N_k^2 n^4)$ , which is asymptotically more favorable than the  $O(N_k^3 n^5)$  scaling of periodic DF-MP2. The corresponding memory cost scales as  $O(N_k^2 n^3)$  for storing the  $U$  amplitudes, which is modest and comparable to that of DF-MP2. Further implementation details of the quartic-scaling periodic drCCD algorithm will be reported elsewhere.<sup>102</sup>

## III. COMPUTATIONAL DETAILS

We have implemented RPA-based LNO-CCSD and LNO-CCSD(T) for both molecular and periodic systems in a developer version of the PYSCF package,<sup>103,104</sup> which employs LIBCINT<sup>105</sup> for Gaussian integral evaluation. The number of Cholesky vectors  $N_{\text{CD}}$  retained in the factorized drCCD equation (22) is chosen sufficiently large to ensure a negligible fitting error,

$$\max \left| \Delta_{\min} \left[ (\Delta_{Iajb})^{-1} - \sum_w^{N_{\text{CD}}} \tau_{iaw} \tau_{jbw} \right] \right| < \tau_{\text{CD}}, \quad (25)$$

where  $\Delta_{\min} = \min \Delta_{Iajb}$  normalizes the fitting error to the interval  $(0, 1]$ . Throughout this work, we adopt  $\tau_{\text{CD}} = 10^{-5}$ , which typically results in  $N_{\text{CD}} = 5–10$  and yields both RPA and SOSEX correlation energy errors below  $10^{-7}$  Ha per atom for both molecules and solids.

For periodic calculations, the integrable divergence of the HF exchange energy is treated using the probe-charge Ewald method,<sup>106</sup> which amounts to shifting the occupied orbital energies downwards by the Madelung constant.<sup>107</sup> Following previous work to achieve optimal finite-size error decay,<sup>24,108</sup> the Madelung-shifted orbital energies are used in periodic MP2, RPA, and the perturbative (T) correction of CCSD(T), whereas the unshifted orbital energies are employed in the periodic CCSD equations. The electron repulsion integrals in periodic systems are handled using the range-separated DF scheme.<sup>109,110</sup>

For the coronene dimer and the anthracene molecular crystal studied in section IV A, we employ standard all-electron cc-pVTZ basis sets<sup>111</sup> together with the corresponding cc-pVTZ-RI fitting basis sets<sup>112</sup> for DF. The [He] core electrons of all non-hydrogen atoms are frozen in correlated calculations. For bulk lithium studied in section IV B, we use GTH-cc-pVDZ and TZ basis sets<sup>113</sup> optimized for the small-core GTH-HF pseudopotentials,<sup>114–116</sup> without freezing any electrons. For bulk copper, also discussed in section IV B, we reoptimized the all-electron cc-pVTZ basis sets following the procedure described in Ref 113 to mitigate severe linear dependencies present in the standard cc-pVTZ sets.<sup>117</sup> The [Ar] core electrons are frozen for Cu. For both metallic systems, density fitting is performed using fitting basis sets optimized according to Ref 112.

In all LNO-CC calculations, we fix the ratio between the occupied and virtual LNO truncation thresholds,  $\gamma = \eta_{\text{occ}}/\eta_{\text{vir}}$ , and vary a single parameter—chosen as  $\eta_{\text{vir}}$ —to control the size of the LAS for approaching the canonical CC limit. For molecular and molecular-crystal systems studied in section IV A, we follow Ref 24 and use  $\gamma = 10$  together with Pipek-Mezey LOs<sup>85,86</sup> constructed using the meta-Löwdin projector.<sup>118</sup> For bulk metals studied in section IV B, we adopt  $\gamma = 1$  and employ intrinsic atomic orbitals<sup>10</sup> as the LOs.

## IV. RESULTS AND DISCUSSION

### A. Noncovalently bound molecules and molecular solids

#### 1. Coronene dimer

Our first test system is the coronene dimer in the parallel-displaced (C2C2PD) configuration taken from the L7 data set.<sup>119</sup> The molecular structure is shown in the inset of fig. 1A. The binding energy  $E_{\text{bind}}$  of C2C2PD has been extensively studied using a range of correlated wavefunction methods, including MP2,<sup>119</sup> RPA,<sup>61</sup> various CC variants,<sup>119–121</sup> and diffusion Monte Carlo<sup>120</sup> (DMC). The current best theoretical estimate is approximately  $-18$  kcal/mol, based on both DMC<sup>120</sup> and CCSD(cT)<sup>121</sup> calculations. (In our convention, a negative  $E_{\text{bind}}$  indicates a stable bound state.) MP2 substantially overestimates the binding energy by about 20 kcal/mol,<sup>61,119</sup> whereas RPA with a HF reference underestimates  $E_{\text{bind}}$  by roughly 6 kcal/mol.<sup>61</sup> Interestingly, despite the severe overbinding at the MP2 level, MP2-based LNO-CCSD(T) has been shown to yield reasonably accurate results for C2C2PD.<sup>120</sup>

In fig. 1A, we compare the convergence of MP2- and RPA-based LNO-CCSD(T) correlation energies for C2C2PD as a function of the maximum LAS size, measured by the number of active LNOs. The data are generated using a sequence of progressively tighter LNO truncation thresholds, starting from  $3 \times 10^{-5}$  and decreasing in steps of approximately half a logarithmic unit (i.e.,  $3 \times 10^{-5}, 10^{-5}, 3 \times 10^{-6}$ , etc.). For a given truncation threshold, RPA-based LNOs yield a slightly smaller LAS size than their MP2-based counterparts, reflect-

ing the screening effect in RPA, which regularizes the magnitude of the drCCD  $T$  amplitudes in the presence of small orbital energy gaps. When the external energy correction  $\Delta E_{\text{c}}^{\text{ext}}$  is not included [eqs. (10) and (14)], the LNO-CCSD(T) correlation energies obtained from MP2- and RPA-based LNOs exhibit very similar convergence behavior with increasing LAS size, indicating that both LNO constructions are of comparable quality for this system. Including  $\Delta E_{\text{c}}^{\text{ext}}$  significantly reduces the energy error for both LNO types and leads to convergence toward the reference value from opposite directions. For comparable LAS sizes, the absolute errors associated with the two LNO types are similar.

In fig. 1B, we show the corresponding convergence behavior of the counterpoise-corrected binding energy  $E_{\text{bind}}$  of C2C2PD, including the HF contribution. Overall, the convergence of  $E_{\text{bind}}$  closely mirrors that of the correlation energy  $E_{\text{c}}$  shown in fig. 1A. An important exception is that employing the RPA-based external correction  $\Delta E_{\text{c}}^{\text{ext}}$  [eq. (14)] leads to noticeably faster convergence of the LNO-CCSD(T) binding energy, reducing the error by approximately a factor of two relative to the MP2-based correction [eq. (10)] for comparable LAS sizes. This behavior is consistent with the aforementioned smaller error of RPA  $E_{\text{lat}}$  compared to MP2. Nevertheless, neither LNO construction achieves chemical accuracy (defined here as an error below 1 kcal/mol) in  $E_{\text{bind}}$  until the LAS size exceeds roughly 600 active LNOs. To further accelerate convergence, we perform a linear extrapolation of  $E_{\text{bind}}$  to the limit  $\Delta E_{\text{c}}^{\text{ext}} = 0$  using the following two-point formula:<sup>122</sup>

$$E_{\text{c,CC}} \approx \frac{E_{\text{c,LNO-CC}}(\eta_1) - E_{\text{c,LNO-CC}}(\eta_2)}{\Delta E_{\text{c}}^{\text{ext}}(\eta_1) - \Delta E_{\text{c}}^{\text{ext}}(\eta_2)}, \quad (26)$$

where  $\eta_1$  and  $\eta_2$  denote two adjacent LNO truncation thresholds separated by approximately half a logarithmic unit. As demonstrated in fig. 1C, this extrapolation scheme is highly effective for both LNO constructions, yielding chemically accurate binding energies with as few as roughly 200 active LNOs, which is only a small fraction of the total orbital count of the system (1776 orbitals).

#### 2. Anthracene crystal

The results in section IV A 1 indicate that RPA-based LNO-CCSD(T) performs on par with the conventional MP2-based approach for noncovalently bound molecular dimers. To extend the assessment to molecular solids, we present in fig. 1D–F the corresponding convergence results for the anthracene molecular crystal with periodic boundary condition using  $\Gamma$ -point Brillouin zone sampling. The unit cell structure is visualized in the inset of fig. 1D. In this case, the binding energy is replaced by the lattice energy, defined as

$$E_{\text{lat}} = \frac{E_{\text{crystal}}}{Z} - E_{\text{mol}} + \Delta E_{\text{CP}}, \quad (27)$$

where  $E_{\text{crystal}}$  is the total energy per unit cell,  $Z$  is the number of molecules per cell,  $E_{\text{mol}}$  is the energy of an isolated molecule, and  $\Delta E_{\text{CP}}$  denotes the counterpoise correction,

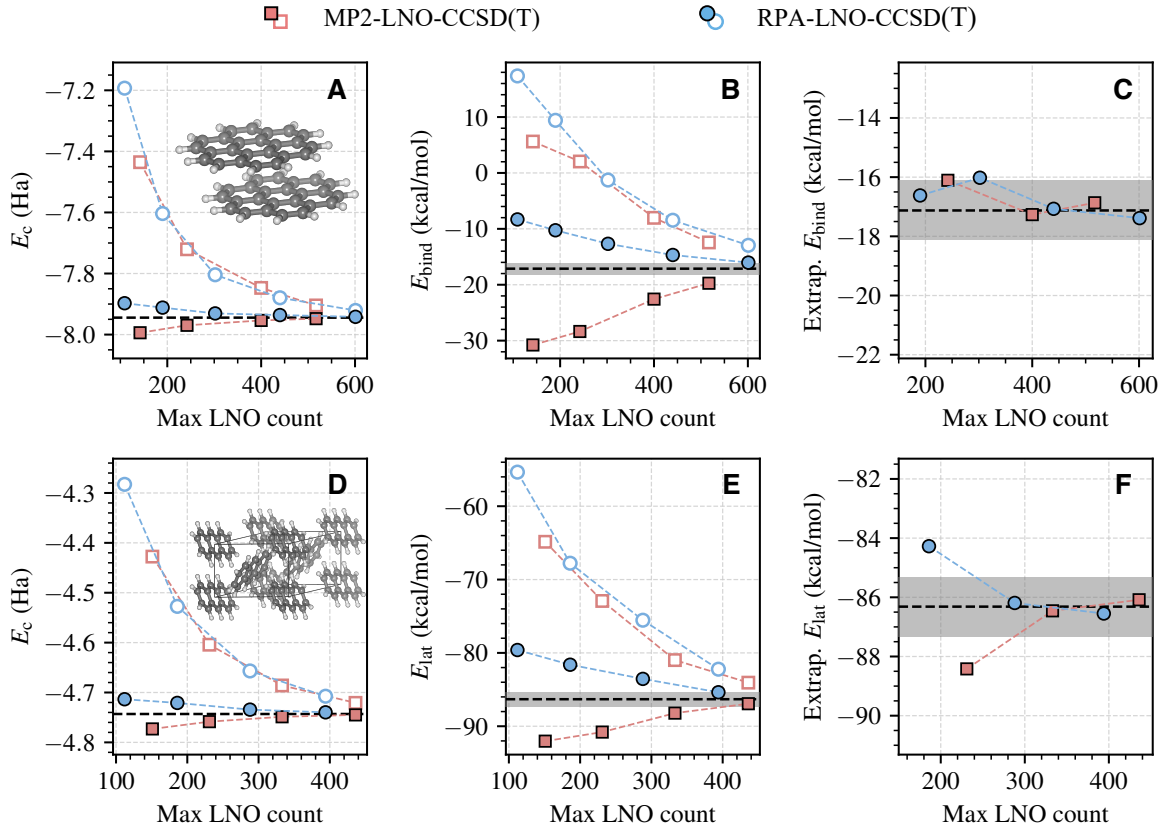


FIG. 1. (A–C) Convergence of MP2- and RPA-based LNO-CCSD(T) correlation energies (A), binding energies (B), and extrapolated binding energies (C) for the coronene dimer in the parallel-displaced (C2C2PD) configuration as a function of the maximum LAS size, measured by the number of active LNOs. (D–F) Corresponding results for the anthracene molecular crystal with  $\Gamma$ -point Brillouin zone sampling, where the lattice energy replaces the binding energy. In (A,B,D,E), open and filled symbols denote LNO-CCSD(T) results obtained without and with the external correction  $\Delta E_c^{\text{ext}}$ , respectively. In (C,F), extrapolated values are obtained using eq. (26) based on two adjacent LNO thresholds; the abscissa indicates the LAS size associated with the tighter threshold. The best estimate of the canonical CCSD(T) result, obtained by averaging the best extrapolations from both MP2- and RPA-based LNO constructions, is shown as a horizontal dashed line in each panel. The gray shaded region in each panel represents an error window of  $\pm 1$  kcal/mol relative to the corresponding reference value. All calculations employ all-electron cc-pVTZ basis sets with the  $1s^2$  core electrons of carbon frozen. The total orbital count (excluding frozen orbitals) is 1776 for C2C2PD and 1120 per unit cell of the anthracene crystal. The binding energy  $E_{\text{bind}}$  and lattice energy  $E_{\text{lat}}$  are counterpoise-corrected.

which we calculated by following previous work.<sup>44</sup> (With this definition, a negative  $E_{\text{lat}}$  corresponds to a stable crystal.) The lattice energies of polyacenes and related molecular crystals have been the subject of numerous recent correlated wavefunction studies,<sup>44,123,124</sup> and periodic LNO-CC methods provide an appealing route to treat such systems.<sup>24</sup>

Compared to the molecular dimer, the overall convergence behavior of the correlation energy (fig. 1D), lattice energy (fig. 1E), and extrapolated lattice energy (fig. 1F) for the anthracene crystal is qualitatively similar to that observed in fig. 1A–C for C2C2PD. A notable exception occurs for the  $\Delta E_c^{\text{ext}}$ -corrected lattice energies in fig. 1E, where the RPA-based results do not exhibit significantly faster convergence than the MP2-based ones, in contrast to the behavior observed for C2C2PD in fig. 1B. This discrepancy is likely an artifact of the  $\Gamma$ -point Brillouin zone sampling, which introduces sizable finite-size errors in the lattice energy. At the  $\Gamma$  point, the MP2 lattice energy is  $-87$  kcal/mol, which fortuitously agrees with our extrapolated CCSD(T) reference value

of  $-86$  kcal/mol (fig. 1F) and appears more accurate than the corresponding RPA result of  $-78$  kcal/mol. The tendency of MP2 to overbind relative to RPA becomes evident only upon employing denser  $k$ -meshes (Table S1), which are currently beyond the reach of our periodic LNO-CCSD(T) implementation. Addressing this limitation is therefore deferred to future work. Nevertheless, the present results demonstrate that RPA-based LNO-CCSD(T) is an attractive alternative to MP2-based LNO-CCSD(T) for noncovalently bound molecules and molecular solids.

## B. Bulk metals

The second class of materials used to assess the performance of RPA-based LNO-CC consists of bulk metals. In these systems, the vanishing band gap and the finite density of states at the Fermi level render MP2 and, more generally, any finite-order perturbation theory formally divergent

in the TDL.<sup>45–47</sup> In practice, however, calculations are always performed in finite simulation cells with discrete  $k$ -point sampling, which introduce an effective finite gap and make MP2 a qualitatively meaningful approximation. Indeed, numerous previous studies have demonstrated the practical success of using MP2-based natural orbitals, wavefunction amplitudes (e.g., through structure-factor analysis<sup>125</sup>), and energy corrections to accelerate CC calculations for metallic systems.<sup>24,78,126–128</sup> Despite these successes, it remains unclear whether RPA-based counterparts can offer tangible advantages over existing MP2-based methods. This question is the focus of the present section.

### 1. BCC Li and FCC Cu with fixed $k$ -point mesh

In fig. 2, we compare the convergence behavior of MP2- and RPA-based LNO-CCSD correlation energies for two representative bulk metals: body-centered cubic (BCC) Li and face-centered cubic (FCC) Cu. In earlier work,<sup>24</sup> MP2-based LNO-CCSD was successfully applied to investigate the ground-state bulk properties of BCC Li. As shown in fig. 2A, replacing MP2 with RPA yields very similar convergence behavior of the LNO-CCSD correlation energy, both with and without  $\Delta E_c^{\text{ext}}$ . The inclusion of  $\Delta E_c^{\text{ext}}$  reduces the absolute correlation energy error, particularly for small LAS sizes. However, this improvement is noticeably less pronounced than that observed for gapped systems [cf. fig. 1(A,D)], consistent with previous findings.<sup>24</sup>

A qualitatively different behavior is observed for FCC Cu, as shown in fig. 2B. While the uncorrected LNO-CCSD correlation energies obtained from MP2- and RPA-based LNOs remain similar, the inclusion of RPA-based  $\Delta E_c^{\text{ext}}$  leads to a substantial reduction in error, achieving an accuracy of approximately 2 kcal/mol with as few as 200 active LNOs. By contrast, achieving comparable accuracy with the MP2-based external correction requires roughly 500 active LNOs. This contrasting behavior can be rationalized by examining the relative performance of MP2 and RPA for the two metallic systems. As summarized in Table S2, RPA significantly overestimates the CCSD correlation energy for Li by about 36%, but only slightly for Cu (about 3%). In contrast, MP2 fortuitously yields a correlation energy close to the CCSD reference for Li for the  $3 \times 3 \times 3$   $k$ -point mesh employed, underestimating it by only about 4%, while substantially overestimating the CCSD reference for Cu by roughly 20%. These trends directly impact the effectiveness of the corresponding external corrections.

To further assess the role of beyond-RPA corrections, we also include in fig. 2 the results for both metals obtained using SOSEX-based LNO-CCSD, which replaces the RPA-based external correction [eq. (14)] with the SOSEX-based one [eq. (17)]. Remarkably, employing the SOSEX-based correction outperforms both MP2- and RPA-based corrections, achieving chemical accuracy for both systems even at the loosest LNO truncation thresholds tested, which corresponds to approximately 50 active LNOs for Li and fewer than 200 for Cu. Interestingly, despite this strong performance as an exter-

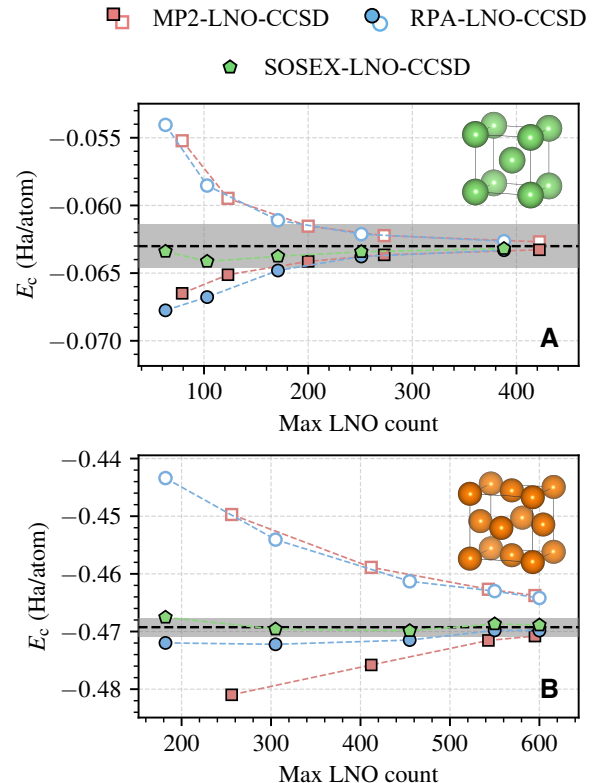


FIG. 2. Convergence of MP2-, RPA-, and SOSEX-based LNO-CCSD correlation energies per atom as a function of the maximum LAS size for (A) body-centered cubic (BCC) Li with a  $3 \times 3 \times 3$   $k$ -mesh and a lattice constant of 3.51 Å, and (B) face-centered cubic (FCC) Cu with a  $2 \times 2 \times 2$   $k$ -mesh and a lattice constant of 3.615 Å. The Li calculations employ the GTH-cc-pVTZ basis sets, while the Cu calculations use the all-electron cc-pVTZ basis sets optimized in this work. Open and filled symbols denote LNO-CCSD results obtained without and with the external energy correction, respectively. The uncorrected SOSEX-based LNO-CCSD results are identical to the uncorrected RPA-based results and are therefore not shown. The best estimate of the canonical CCSD correlation energy, obtained by averaging the best extrapolated values from all three methods using eq. (26), is indicated by a horizontal dashed line in each panel. The gray shaded region represents an error window of  $\pm 1$  kcal/mol relative to the corresponding reference value.

nal correction, SOSEX itself is not a particularly accurate approximation to the CCSD correlation energy, systematically underestimating it by about 20% for both metals. Taken together, these results underscore that the effectiveness of LNO-CC hinges not only on the quality of the LNOs, but also critically on the choice of the external energy correction.

### 2. BCC Li with enlarging $k$ -point meshes

The results discussed in section IV B 1 were obtained at fixed  $k$ -point meshes and may therefore be affected by finite-size errors. This issue is particularly relevant for MP2-based treatments, whose accuracy is expected to degrade as the TDL is approached. To systematically assess the behavior of differ-

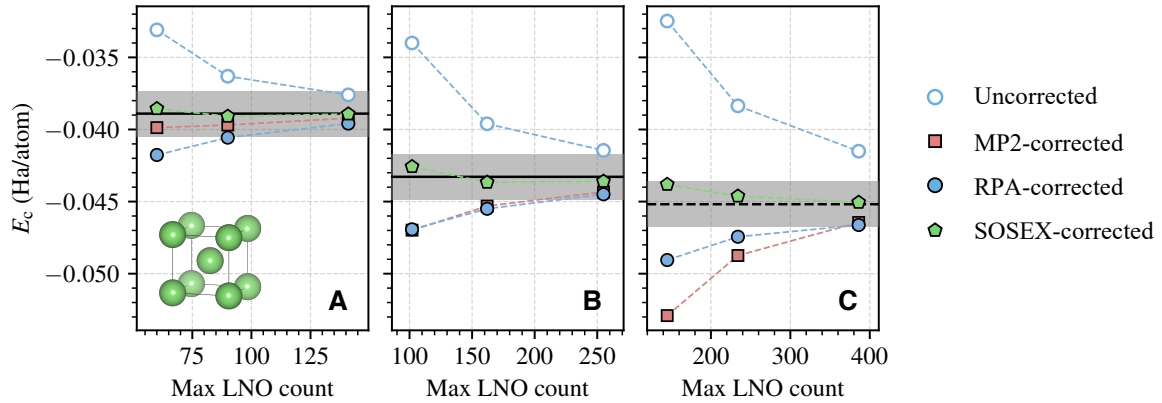


FIG. 3. Convergence of LNO-CCSD correlation energies for BCC Li as a function of the maximum LAS size using RPA-derived LNOs with different external corrections  $\Delta E_c^{\text{ext}}$ , for (A)  $2 \times 2 \times 2$ , (B)  $3 \times 3 \times 3$ , and (C)  $4 \times 4 \times 4$   $k$ -point meshes. All  $k$ -meshes are shifted from the  $\Gamma$  point by  $\mathbf{k}^* = \frac{2\pi}{L}(\frac{1}{4}, \frac{1}{4}, \frac{1}{4})$ , where  $L = N_k^{1/3}a$  and  $a = 3.51 \text{ \AA}$  is the lattice constant. All calculations employ the GTH-cc-pVDZ basis sets. In panels (A) and (B), the horizontal solid lines indicate reference values obtained from canonical  $k$ -point CCSD calculations. In panel (C), the horizontal dashed line denotes our best extrapolated estimate obtained using eq. (26) with the SOSEX external correction [eq. (17)]. The gray shaded region in each panel represents an error window of  $\pm 1 \text{ kcal/mol}$  relative to the corresponding reference value.

ent low-level theories with respect to  $k$ -point convergence, we repeated the LNO-CCSD calculations for BCC Li using progressively denser  $k$ -point meshes, from  $2 \times 2 \times 2$  to  $4 \times 4 \times 4$ , employing the smaller GTH-cc-pVDZ basis sets. In these calculations, the RPA-derived LNOs are kept fixed, and we focus exclusively on comparing the impact of different choices of the external correction. The results obtained for three representative LNO truncation thresholds ( $3 \times 10^{-4}$ ,  $10^{-4}$ , and  $3 \times 10^{-5}$ ) are summarized in fig. 3.

As the  $k$ -point mesh becomes denser, the error of the uncorrected LNO-CCSD results increases at each truncation threshold, even though the corresponding LAS sizes continue to grow. This behavior reflects the slow decay of the long-range correlation energy in metallic systems and highlights the necessity of incorporating an appropriate external correction. With the relatively coarse  $2 \times 2 \times 2$   $k$ -mesh, the MP2-based correction yields rapid convergence with the LAS size. However, its performance deteriorates markedly as the  $k$ -mesh is refined. For the largest  $4 \times 4 \times 4$  mesh, the MP2-based correction provides only marginal improvement in the absolute error over the uncorrected results. In contrast, both RPA- and SOSEX-based external corrections yield results that are stable across different  $k$ -point meshes. At the  $4 \times 4 \times 4$   $k$ -mesh, the RPA-based external correction clearly outperforms the MP2-based counterpart. For all  $k$ -meshes considered, the RPA-corrected LNO-CCSD attains chemical accuracy when using the tightest threshold tested ( $3 \times 10^{-5}$ ). Remarkably, the SOSEX-corrected LNO-CCSD achieves chemical accuracy even with the loosest threshold ( $10^{-4}$ ), reducing the required LAS size by approximately a factor of three relative to the RPA-based correction. The superior performance of the SOSEX-based external correction is consistent with the trends observed earlier in fig. 2 for fixed  $k$ -meshes.

## V. CONCLUSION

In this work, we have developed RPA as a promising alternative to MP2 as the low-level theory within the LNO-CC framework, by leveraging the drCCD formulation of RPA. Our numerical benchmarks on noncovalently bound molecules, molecular solids, and bulk metals demonstrate that RPA-derived natural orbitals are of comparable quality to their MP2-based counterparts for describing short-range electron correlation. In contrast, composite energy corrections based on RPA and the closely related SOSEX approximation systematically outperform those based on MP2, with particularly pronounced improvements for metallic systems as the TDL is approached. These results highlight the critical importance of a judiciously chosen low-level theory for the practical performance of fragment embedding and local correlation methods.

Several avenues for future work naturally follow from the present study. First, beyond the encouraging numerical results reported here, a deeper theoretical understanding of why certain composite corrections—most notably SOSEX—perform substantially better than others would be highly valuable. Second, in addition to SOSEX, other beyond-RPA approaches that incorporate exchange effects<sup>80,129</sup> or higher-order contributions<sup>96,130</sup> offer promising opportunities to further enhance the accuracy and robustness of LNO-CC. Finally, the RPA-based strategy presented in this work is general and can be straightforwardly extended to other MP2-based fragment embedding and local correlation frameworks. With continued methodological developments along these lines, we anticipate that RPA and its extensions will play an increasingly important role in enabling accurate and efficient high-level quantum chemical calculations for complex molecular and condensed-phase systems.

## SUPPORTING INFORMATION

See the Supporting Information for (i) detailed basis-set information, (ii) lattice energies of anthracene computed at the HF, MP2, and RPA levels, and (iii) correlation energies of BCC Li and FCC Cu obtained using MP2, RPA, SOSEX, and CCSD.

## CONFLICT OF INTEREST

The authors declare no competing conflicts of interest.

## DATA AVAILABILITY

The data that support the findings of this study are available from the corresponding author upon reasonable request.

## ACKNOWLEDGMENTS

This work was supported by the startup funds from the University of Maryland, College Park. We acknowledge computing resources provided by the Division of Information Technology at the University of Maryland, College Park, as well as by the National Science Foundation through the ACCESS program under allocation CHE240210.

- <sup>1</sup>R. J. Bartlett and M. Musiał, “Coupled-cluster theory in quantum chemistry,” *Rev. Mod. Phys.* **79**, 291–352 (2007).
- <sup>2</sup>Q. Sun and G. K.-L. Chan, “Quantum embedding theories,” *Acc. Chem. Res.* **49**, 2705–2712 (2016).
- <sup>3</sup>J. M. Herbert, “Fantasy versus reality in fragment-based quantum chemistry,” *J. Chem. Phys.* **151**, 170901 (2019).
- <sup>4</sup>S. J. R. Lee, M. Welborn, F. R. Manby, and T. F. I. Miller, “Projection-based wavefunction-in-dft embedding,” *Acc. Chem. Res.* **52**, 1359–1368 (2019).
- <sup>5</sup>A. Wasserman and M. Pavanello, “Quantum embedding electronic structure methods,” *Int. J. Quantum Chem.* **120**, e26495 (2020).
- <sup>6</sup>F. R. Manby, M. Stella, J. D. Goodpaster, and T. F. I. Miller, “A simple, exact density-functional-theory embedding scheme,” *J. Chem. Theory Comput.* **8**, 2564–2568 (2012).
- <sup>7</sup>C. Daday, C. König, J. Neugebauer, and C. Filippi, “Wavefunction in density functional theory embedding for excited states: Which wavefunctions, which densities?” *Chem. Phys. Chem.* **15**, 3205–3217 (2014).
- <sup>8</sup>C. R. Jacob and J. Neugebauer, “Subsystem density-functional theory,” *Wiley Interdiscip. Rev. Comput. Mol. Sci.* **4**, 325–362 (2014).
- <sup>9</sup>F. Libisch, C. Huang, and E. A. Carter, “Embedded correlated wavefunction schemes: Theory and applications,” *Acc. Chem. Res.* **47**, 2768–2775 (2014).
- <sup>10</sup>G. Knizia and G. K.-L. Chan, “Density matrix embedding: A strong-coupling quantum embedding theory,” *J. Chem. Theory Comput.* **9**, 1428–1432 (2013).
- <sup>11</sup>S. Wouters, C. A. Jiménez-Hoyos, Q. Sun, and G. K.-L. Chan, “A practical guide to density matrix embedding theory in quantum chemistry,” *J. Chem. Theory Comput.* **12**, 2706–2719 (2016).
- <sup>12</sup>Z.-H. Cui, T. Zhu, and G. K.-L. Chan, “Efficient implementation of ab initio quantum embedding in periodic systems: Density matrix embedding theory,” *J. Chem. Theory Comput.* **16**, 119–129 (2020).
- <sup>13</sup>H.-Z. Ye, N. D. Ricke, H. K. Tran, and T. Van Voorhis, “Bootstrap embedding for molecules,” *J. Chem. Theory Comput.* **15**, 4497–4506 (2019).
- <sup>14</sup>M. Cho, O. R. Meitei, L. P. Weisburn, O. Weser, S. Weatherly, A. Alexiu, R. Hanscam, H. K. Tran, H.-Z. Ye, M. Welborn, N. Ricke, T. Tsuchimochi, A. Trofimov, T. Orkhon, N. Whelpley, C. Luo, and T. Van Voorhis, “Quemb: A toolbox for bootstrap embedding calculations of molecular and periodic systems,” *J. Phys. Chem. A* **129**, 6538–6551 (2025).
- <sup>15</sup>M. Nusspickel and G. H. Booth, “Systematic improbability in quantum embedding for real materials,” *Phys. Rev. X* **12**, 011046 (2022).
- <sup>16</sup>A. Shee, F. M. Faulstich, K. B. Whaley, L. Lin, and M. Head-Gordon, “A static quantum embedding scheme based on coupled cluster theory,” *J. Chem. Phys.* **161**, 164107 (2024).
- <sup>17</sup>M. R. Hermes, R. Pandharkar, and L. Gagliardi, “Variational localized active space self-consistent field method,” *J. Chem. Theory Comput.* **16**, 4923–4937 (2020).
- <sup>18</sup>D. S. King, B. Jangid, M. R. Hermes, and L. Gagliardi, “Bridging the gap between molecules and materials in quantum chemistry with localized active spaces,” *Nat. Commun.* **16**, 10832 (2025).
- <sup>19</sup>Z. Rolik and M. Kállay, “A general-order local coupled-cluster method based on the cluster-in-molecule approach,” *J. Chem. Phys.* **135**, 104111 (2011).
- <sup>20</sup>Z. Rolik, L. Szegedy, I. Ladányszki, B. Ládóczki, and M. Kállay, “An efficient linear-scaling CCSD(T) method based on local natural orbitals,” *J. Chem. Phys.* **139**, 094105 (2013).
- <sup>21</sup>P. R. Nagy and M. Kállay, “Optimization of the linear-scaling local natural orbital CCSD(T) method: Redundancy-free triples correction using Laplace transform,” *J. Chem. Phys.* **146**, 214106 (2017).
- <sup>22</sup>P. R. Nagy and M. Kállay, “Approaching the basis set limit of ccsd(t) energies for large molecules with local natural orbital coupled-cluster methods,” *J. Chem. Theory Comput.* **15**, 5275–5298 (2019).
- <sup>23</sup>P. R. Nagy, “State-of-the-art local correlation methods enable affordable gold standard quantum chemistry for up to hundreds of atoms,” *Chem. Sci.* **15**, 14556–14584 (2024).
- <sup>24</sup>H.-Z. Ye and T. C. Berkelbach, “Periodic local coupled-cluster theory for insulators and metals,” *J. Chem. Theory Comput.* **20**, 8948–8959 (2024).
- <sup>25</sup>S. Li, J. Ma, and Y. Jiang, “Linear scaling local correlation approach for solving the coupled cluster equations of large systems,” *J. Comput. Chem.* **23**, 237–244 (2002).
- <sup>26</sup>W. Li and S. Li, “Divide-and-conquer local correlation approach to the correlation energy of large molecules,” *J. Chem. Phys.* **121**, 6649–6657 (2004).
- <sup>27</sup>S. Li, J. Shen, W. Li, and Y. Jiang, “An efficient implementation of the “cluster-in-molecule” approach for local electron correlation calculations,” *J. Chem. Phys.* **125**, 074109 (2006).
- <sup>28</sup>W. Li, P. Piecuch, J. R. Gour, and S. Li, “Local correlation calculations using standard and renormalized coupled-cluster approaches,” *J. Chem. Phys.* **131**, 114109 (2009).
- <sup>29</sup>Y. Wang, Z. Ni, W. Li, and S. Li, “Cluster-in-molecule local correlation approach for periodic systems,” *J. Chem. Theory Comput.* **15**, 2933–2943 (2019).
- <sup>30</sup>Y. Wang, Z. Ni, F. Neese, W. Li, Y. Guo, and S. Li, “Cluster-in-molecule method combined with the domain-based local pair natural orbital approach for electron correlation calculations of periodic systems,” *J. Chem. Theory Comput.* **18**, 6510–6521 (2022).
- <sup>31</sup>C. Møller and M. S. Plesset, “Note on an approximation treatment for many-electron systems,” *Phys. Rev.* **46**, 618–622 (1934).
- <sup>32</sup>F. Neese, A. Hansen, and D. G. Liakos, “Efficient and accurate approximations to the local coupled cluster singles doubles method using a truncated pair natural orbital basis,” *J. Chem. Phys.* **131**, 064103 (2009).
- <sup>33</sup>F. Neese, F. Wennmohs, and A. Hansen, “Efficient and accurate local approximations to coupled-electron pair approaches: An attempt to revive the pair natural orbital method,” *J. Chem. Phys.* **130**, 114108 (2009).
- <sup>34</sup>A. Hansen, D. G. Liakos, and F. Neese, “Efficient and accurate local single reference correlation methods for high-spin open-shell molecules using pair natural orbitals,” *J. Chem. Phys.* **135**, 214102 (2011).
- <sup>35</sup>L. M. J. Huntington, A. Hansen, F. Neese, and M. Nooijen, “Accurate thermochemistry from a parameterized coupled-cluster singles and doubles model and a local pair natural orbital based implementation for applications to larger systems,” *J. Chem. Phys.* **136**, 064101 (2012).
- <sup>36</sup>D. G. Liakos, M. Sparta, M. K. Kesharwani, J. M. L. Martin, and F. Neese, “Exploring the accuracy limits of local pair natural orbital coupled-cluster theory,” *J. Chem. Theory Comput.* **11**, 1525–1539 (2015).

<sup>37</sup>H.-J. Werner and M. Schütz, “An efficient local coupled cluster method for accurate thermochemistry of large systems,” *J. Chem. Phys.* **135**, 144116 (2011).

<sup>38</sup>M. Nusspickel, B. Ibrahim, and G. H. Booth, “Effective reconstruction of expectation values from ab initio quantum embedding,” *J. Chem. Theory Comput.* **19**, 2769–2791 (2023).

<sup>39</sup>J. Li and T. Zhu, “Interacting-bath dynamical embedding for capturing nonlocal electron correlation in solids,” *Phys. Rev. Lett.* **133**, 216402 (2024).

<sup>40</sup>H.-Z. Ye and T. Van Voorhis, “Atom-based bootstrap embedding for molecules,” *J. Phys. Chem. Lett.* **10**, 6368–6374 (2019).

<sup>41</sup>R. A. Distasio JR. and M. Head-Gordon, “Optimized spin-component scaled second-order Møller-Plesset perturbation theory for intermolecular interaction energies,” *Mol. Phys.* **105**, 1073–1083 (2007).

<sup>42</sup>S. M. Cybulski and M. L. Lytle, “The origin of deficiency of the supermolecule second-order Møller-Plesset approach for evaluating interaction energies,” *J. Chem. Phys.* **127**, 141102 (2007).

<sup>43</sup>G. J. O. Beran, “Modeling polymorphic molecular crystals with electronic structure theory,” *Chem. Rev.* **116**, 5567–5613 (2016).

<sup>44</sup>Y. H. Liang, H.-Z. Ye, and T. C. Berkelbach, “Can spin-component scaled mp2 achieve kj/mol accuracy for cohesive energies of molecular crystals?” *J. Phys. Chem. Lett.* **14**, 10435–10441 (2023).

<sup>45</sup>J. J. Shepherd and A. Grüneis, “Many-body quantum chemistry for the electron gas: Convergent perturbative theories,” *Phys. Rev. Lett.* **110**, 226401 (2013).

<sup>46</sup>N. Masiros, A. Irmler, T. Schäfer, and A. Grüneis, “Averting the infrared catastrophe in the gold standard of quantum chemistry,” *Phys. Rev. Lett.* **131**, 186401 (2023).

<sup>47</sup>V. A. Neufeld and T. C. Berkelbach, “Highly accurate electronic structure of metallic solids from coupled-cluster theory with nonperturbative triple excitations,” *Phys. Rev. Lett.* **131**, 186402 (2023).

<sup>48</sup>D. Bohm and D. Pines, “A collective description of electron interactions: Iii. coulomb interactions in a degenerate electron gas,” *Phys. Rev.* **92**, 609–625 (1953).

<sup>49</sup>M. Gell-Mann and K. A. Brueckner, “Correlation energy of an electron gas at high density,” *Phys. Rev.* **106**, 364–368 (1957).

<sup>50</sup>F. Furche, “Molecular tests of the random phase approximation to the exchange-correlation energy functional,” *Phys. Rev. B* **64**, 195120 (2001).

<sup>51</sup>X. Ren, P. Rinke, C. Joas, and M. Scheffler, “Random-phase approximation and its applications in computational chemistry and materials science,” *J. Mater. Sci.* **47**, 7447–7471 (2012).

<sup>52</sup>G. P. Chen, V. K. Voora, M. M. Agee, S. G. Balasubramani, and F. Furche, “Random-phase approximation methods,” *Ann. Rev. Phys. Chem.* **68**, 421–445 (2017).

<sup>53</sup>I. Y. Zhang and X. Xu, “On the top rung of jacob’s ladder of density functional theory: Toward resolving the dilemma of sie and nce,” *Wiley Interdiscip. Rev. Comput. Mol. Sci.* **11**, e1490 (2021).

<sup>54</sup>J. Harl and G. Kresse, “Cohesive energy curves for noble gas solids calculated by adiabatic connection fluctuation-dissipation theory,” *Phys. Rev. B* **77**, 045136 (2008).

<sup>55</sup>D. Lu, Y. Li, D. Rocca, and G. Galli, “Ab initio calculation of van der waals bonded molecular crystals,” *Phys. Rev. Lett.* **102**, 206411 (2009).

<sup>56</sup>M. Del Ben, J. Hutter, and J. VandeVondele, “Electron correlation in the condensed phase from a resolution of identity approach based on the gaussian and plane waves scheme,” *J. Chem. Theory Comput.* **9**, 2654–2671 (2013).

<sup>57</sup>J. Klimeš, “Lattice energies of molecular solids from the random phase approximation with singles corrections,” *J. Chem. Phys.* **145**, 094506 (2016).

<sup>58</sup>Y. Yao and Y. Kanai, “Nuclear quantum effect and its temperature dependence in liquid water from random phase approximation via artificial neural network,” *J. Phys. Chem. Lett.* **12**, 6354–6362 (2021).

<sup>59</sup>M. Hellgren and L. Baguet, “Random phase approximation with exchange for an accurate description of crystalline polymorphism,” *Phys. Rev. Res.* **3**, 033263 (2021).

<sup>60</sup>K. N. Pham, M. Modrzejewski, and J. Klimeš, “Assessment of random phase approximation and second-order Møller-Plesset perturbation theory for many-body interactions in solid ethane, ethylene, and acetylene,” *J. Chem. Phys.* **158**, 144119 (2023).

<sup>61</sup>Y. H. Liang, X. Zhang, G. K.-L. Chan, T. C. Berkelbach, and H.-Z. Ye, “Efficient implementation of the random phase approximation with domain-based local pair natural orbitals,” *J. Chem. Theory Comput.* **21**, 2918–2927 (2025).

<sup>62</sup>X. Ren, P. Rinke, and M. Scheffler, “Exploring the random phase approximation: Application to co adsorbed on cu(111),” *Phys. Rev. B* **80**, 045402 (2009).

<sup>63</sup>J. Harl and G. Kresse, “Accurate bulk properties from approximate many-body techniques,” *Phys. Rev. Lett.* **103**, 056401 (2009).

<sup>64</sup>L. Schimka, J. Harl, A. Stroppa, A. Grüneis, M. Marsman, F. Mittendorfer, and G. Kresse, “Accurate surface and adsorption energies from many-body perturbation theory,” *Nature Mater.* **9**, 741–744 (2010).

<sup>65</sup>T. Olsen, J. Yan, J. J. Mortensen, and K. S. Thygesen, “Dispersive and covalent interactions between graphene and metal surfaces from the random phase approximation,” *Phys. Rev. Lett.* **107**, 156401 (2011).

<sup>66</sup>M. Rohlfing and T. Bredow, “Binding energy of adsorbates on a noble-metal surface: Exchange and correlation effects,” *Phys. Rev. Lett.* **101**, 266106 (2008).

<sup>67</sup>J. Ma, A. Michaelides, D. Alfè, L. Schimka, G. Kresse, and E. Wang, “Adsorption and diffusion of water on graphene from first principles,” *Phys. Rev. B* **84**, 033402 (2011).

<sup>68</sup>H.-J. Kim, A. Tkatchenko, J.-H. Cho, and M. Scheffler, “Benzene adsorbed on si(001): The role of electron correlation and finite temperature,” *Phys. Rev. B* **85**, 041403 (2012).

<sup>69</sup>P. S. Schmidt and K. S. Thygesen, “Benchmark database of transition metal surface and adsorption energies from many-body perturbation theory,” *J. Phys. Chem. C* **122**, 4381–4390 (2018).

<sup>70</sup>C. Sheldon, J. Paier, D. Usyat, and J. Sauer, “Hybrid rpa:dft approach for adsorption on transition metal surfaces: Methane and ethane on platinum (111),” *J. Chem. Theory Comput.* **20**, 2219–2227 (2024).

<sup>71</sup>F. Aryasetiawan, M. Imada, A. Georges, G. Kotliar, S. Biermann, and A. I. Lichtenstein, “Frequency-dependent local interactions and low-energy effective models from electronic structure calculations,” *Phys. Rev. B* **70**, 195104 (2004).

<sup>72</sup>E. Şəsioglu, C. Friedrich, and S. Blügel, “Effective coulomb interaction in transition metals from constrained random-phase approximation,” *Phys. Rev. B* **83**, 121101 (2011).

<sup>73</sup>Y. Chang, E. G. C. P. van Loon, B. Eskridge, B. Busemeyer, M. A. Morales, C. E. Dreyer, A. J. Millis, S. Zhang, T. O. Wehling, L. K. Wagner, and M. Rönsler, “Downfolding from ab initio to interacting model hamiltonians: comprehensive analysis and benchmarking of the dft+rpa approach,” *npj Comput. Mater.* **10**, 129 (2024).

<sup>74</sup>C. J. C. Scott and G. H. Booth, “Rigorous screened interactions for realistic correlated electron systems,” *Phys. Rev. Lett.* **132**, 076401 (2024).

<sup>75</sup>B. Ramberger, Z. Sukurma, T. Schäfer, and G. Kresse, “Rpa natural orbitals and their application to post-hartree-fock electronic structure methods,” *J. Chem. Phys.* **151**, 214106 (2019).

<sup>76</sup>T. Schäfer, F. Libisch, G. Kresse, and A. Grüneis, “Local embedding of coupled cluster theory into the random phase approximation using plane waves,” *J. Chem. Phys.* **154**, 011101 (2021).

<sup>77</sup>T. Schäfer, A. Gallo, A. Irmler, F. Hummel, and A. Grüneis, “Surface science using coupled cluster theory via local wannier functions and in-rpa-embedding: The case of water on graphitic carbon nitride,” *J. Chem. Phys.* **155**, 244103 (2021).

<sup>78</sup>J. M. Callahan, M. F. Lange, and T. C. Berkelbach, “Dynamical correlation energy of metals in large basis sets from downfolding and composite approaches,” *J. Chem. Phys.* **154**, 211105 (2021).

<sup>79</sup>G. E. Scuseria, T. M. Henderson, and D. C. Sorensen, “The ground state correlation energy of the random phase approximation from a ring coupled cluster doubles approach,” *J. Chem. Phys.* **129**, 231101 (2008).

<sup>80</sup>A. Heßelmann, “Random-phase-approximation correlation method including exchange interactions,” *Phys. Rev. A* **85**, 012517 (2012).

<sup>81</sup>M. Kállay, “Linear-scaling implementation of the direct random-phase approximation,” *J. Chem. Phys.* **142**, 204105 (2015).

<sup>82</sup>H.-Z. Ye and T. C. Berkelbach, “Ab Initio surface chemistry with chemical accuracy: Application to water on metal oxides,” arXiv preprint arXiv:2309.14640 (2023).

<sup>83</sup>H.-Z. Ye and T. C. Berkelbach, “Adsorption and vibrational spectroscopy of co on the surface of mgo from periodic local coupled-cluster theory,” *Faraday Discuss.* , – (2024).

<sup>84</sup>A. Grüneis, M. Marsman, J. Harl, L. Schimka, and G. Kresse, “Making the random phase approximation to electronic correlation accurate,” *J. Chem.*

**Phys.** **131**, 154115 (2009).

<sup>85</sup>J. Pipek and P. G. Mezey, “A fast intrinsic localization procedure applicable for ab initio and semiempirical linear combination of atomic orbital wave functions,” **J. Chem. Phys.** **90**, 4916–4926 (1989).

<sup>86</sup>E. O. Jónsson, S. Lehtola, M. Puska, and H. Jónsson, “Theory and applications of generalized pipek-mezey wannier functions,” **J. Chem. Theory Comput.** **13**, 460–474 (2017).

<sup>87</sup>S. F. Boys, “Construction of some molecular orbitals to be approximately invariant for changes from one molecule to another,” **Rev. Mod. Phys.** **32**, 296–299 (1960).

<sup>88</sup>N. Marzari, A. A. Mostofi, J. R. Yates, I. Souza, and D. Vanderbilt, “Maximally localized wannier functions: Theory and applications,” **Rev. Mod. Phys.** **84**, 1419–1475 (2012).

<sup>89</sup>A. Ekert and P. L. Knight, “Entangled quantum systems and the schmidt decomposition,” **Am. J. Phys.** **63**, 415–423 (1995).

<sup>90</sup>H. D. Cornean, D. Gontier, A. Levitt, and D. Monaco, “Localised wannier functions in metallic systems,” **Ann. Henri Poincaré** **20**, 1367–1391 (2019).

<sup>91</sup>T. M. Henderson and G. E. Scuseria, “The connection between self-interaction and static correlation: a random phase approximation perspective,” **Mol. Phys.** **108**, 2511–2517 (2010).

<sup>92</sup>G. E. Scuseria, T. M. Henderson, and I. W. Bulik, “Particle-particle and quasiparticle random phase approximations: Connections to coupled cluster theory,” **J. Chem. Phys.** **139**, 104113 (2013).

<sup>93</sup>D. Peng, S. N. Steinmann, H. van Aggelen, and W. Yang, “Equivalence of particle-particle random phase approximation correlation energy and ladder-coupled-cluster doubles,” **J. Chem. Phys.** **139**, 104112 (2013).

<sup>94</sup>J. Rekkedal, S. Coriani, M. F. Iozzi, A. M. Teale, T. Helgaker, and T. B. Pedersen, “Communication: Analytic gradients in the random-phase approximation,” **J. Chem. Phys.** **139**, 081101 (2013).

<sup>95</sup>R. Song, X. Gong, and H.-Z. Ye, “Unphysical solutions in coupled-cluster-based random phase approximation and how to avoid them,” **J. Chem. Phys.** **163**, 161103 (2025).

<sup>96</sup>J. J. Shepherd, T. M. Henderson, and G. E. Scuseria, “Coupled cluster channels in the homogeneous electron gas,” **J. Chem. Phys.** **140**, 124102 (2014).

<sup>97</sup>H. Koch and A. Sánchez de Merás, “Size-intensive decomposition of orbital energy denominators,” **J. Chem. Phys.** **113**, 508–513 (2000).

<sup>98</sup>F. Aquilante, L. Boman, J. Boström, H. Koch, R. Lindh, A. S. de Merás, and T. B. Pedersen, “Cholesky decomposition techniques in electronic structure theory,” in *Linear-Scaling Techniques in Computational Chemistry and Physics: Methods and Applications*, edited by R. Zalesny, M. G. Papadopoulos, P. G. Mezey, and J. Leszczynski (Springer Netherlands, Dordrecht, 2011) pp. 301–343.

<sup>99</sup>J. L. Whitten, “Coulombic potential energy integrals and approximations,” **J. Chem. Phys.** **58**, 4496–4501 (1973).

<sup>100</sup>M. Feyereisen, G. Fitzgerald, and A. Komornicki, “Use of approximate integrals in ab initio theory. an application in mp2 energy calculations,” **Chem. Phys. Lett.** **208**, 359–363 (1993).

<sup>101</sup>B. I. Dunlap, “Robust and variational fitting,” **Phys. Chem. Chem. Phys.** **2**, 2113–2116 (2000).

<sup>102</sup>X. Gong, R. Song, and H.-Z. Ye, In preparation.

<sup>103</sup>Q. Sun, T. C. Berkelbach, N. S. Blunt, G. H. Booth, S. Guo, Z. Li, J. Liu, J. D. McClain, E. R. Sayfutyarova, S. Sharma, S. Wouters, and G. K.-L. Chan, “PySCF: the python-based simulations of chemistry framework,” **Wiley Interdiscip. Rev. Comput. Mol. Sci.** **8**, e1340 (2018).

<sup>104</sup>Q. Sun, X. Zhang, S. Banerjee, P. Bao, M. Barbry, N. S. Blunt, N. A. Bogdanov, G. H. Booth, J. Chen, Z.-H. Cui, J. J. Eriksen, Y. Gao, S. Guo, J. Hermann, M. R. Hermes, K. Koh, P. Koval, S. Lehtola, Z. Li, J. Liu, N. Mardirossian, J. D. McClain, M. Motta, B. Mussard, H. Q. Pham, A. Pulkkin, W. Purwanto, P. J. Robinson, E. Ronca, E. R. Sayfutyarova, M. Scheurer, H. F. Schurkus, J. E. T. Smith, C. Sun, S.-N. Sun, S. Upadhyay, L. K. Wagner, X. Wang, A. White, J. D. Whitfield, M. J. Williamson, S. Wouters, J. Yang, J. M. Yu, T. Zhu, T. C. Berkelbach, S. Sharma, A. Y. Sokolov, and G. K.-L. Chan, “Recent developments in the PySCF program package,” **J. Chem. Phys.** **153**, 024109 (2020).

<sup>105</sup>Q. Sun, “Libcint: An efficient general integral library for gaussian basis functions,” **J. Comput. Chem.** **36**, 1664–1671 (2015).

<sup>106</sup>J. Paier, R. Hirschl, M. Marsman, and G. Kresse, “The perdew–burke–ernzerhof exchange-correlation functional applied to the g2-1 test set using a plane-wave basis set,” **J. Chem. Phys.** **122**, 234102 (2005).

<sup>107</sup>P. Broqvist, A. Alkauskas, and A. Pasquarello, “Hybrid-functional calculations with plane-wave basis sets: Effect of singularity correction on total energies, energy eigenvalues, and defect energy levels,” **Phys. Rev. B** **80**, 085114 (2009).

<sup>108</sup>X. Xing and L. Lin, “Inverse volume scaling of finite-size error in periodic coupled cluster theory,” **Phys. Rev. X** **14**, 011059 (2024).

<sup>109</sup>H.-Z. Ye and T. C. Berkelbach, “Fast periodic Gaussian density fitting by range separation,” **J. Chem. Phys.** **154**, 131104 (2021).

<sup>110</sup>H.-Z. Ye and T. C. Berkelbach, “Tight distance-dependent estimators for screening two-center and three-center short-range Coulomb integrals over Gaussian basis functions,” **J. Chem. Phys.** **155**, 124106 (2021).

<sup>111</sup>T. H. Dunning, “Gaussian basis sets for use in correlated molecular calculations. i. the atoms boron through neon and hydrogen,” **J. Chem. Phys.** **90**, 1007–1023 (1989).

<sup>112</sup>F. Weigend, “A fully direct ri-hf algorithm: Implementation, optimised auxiliary basis sets, demonstration of accuracy and efficiency,” **Phys. Chem. Chem. Phys.** **4**, 4285–4291 (2002).

<sup>113</sup>H.-Z. Ye and T. C. Berkelbach, “Correlation-consistent gaussian basis sets for solids made simple,” **J. Chem. Theory Comput.** **18**, 1595–1606 (2022).

<sup>114</sup>S. Goedecker, M. Teter, and J. Hutter, “Separable dual-space gaussian pseudopotentials,” **Phys. Rev. B** **54**, 1703–1710 (1996).

<sup>115</sup>C. Hartwigsen, S. Goedecker, and J. Hutter, “Relativistic separable dual-space gaussian pseudopotentials from h to rn,” **Phys. Rev. B** **58**, 3641–3662 (1998).

<sup>116</sup>J. Hutter, “New optimization of GTH pseudopotentials for PBE, SCAN, PBE0 functionals. GTH pseudopotentials for Hartree-Fock. NLCC pseudopotentials for PBE.” <https://github.com/juerghutter/GTH> (2019).

<sup>117</sup>N. B. Balabanov and K. A. Peterson, “Systematically convergent basis sets for transition metals. i. all-electron correlation consistent basis sets for the 3d elements sc-zn,” **J. Chem. Phys.** **123**, 064107 (2005).

<sup>118</sup>Q. Sun and G. K.-L. Chan, “Exact and optimal quantum mechanics/molecular mechanics boundaries,” **J. Chem. Theory Comput.** **10**, 3784–3790 (2014).

<sup>119</sup>R. Sedlak, T. Janowski, M. Pitoňák, J. Řezáč, P. Pulay, and P. Hobza, “Accuracy of quantum chemical methods for large noncovalent complexes,” **J. Chem. Theory Comput.** **9**, 3364–3374 (2013).

<sup>120</sup>Y. S. Al-Hamdan, P. R. Nagy, A. Zen, D. Barton, M. Kállay, J. G. Brandenburg, and A. Tkatchenko, “Interactions between large molecules pose a puzzle for reference quantum mechanical methods,” **Nat. Commun.** **12**, 3927 (2021).

<sup>121</sup>T. Schäfer, A. Irmller, A. Gallo, and A. Grüneis, “Understanding discrepancies in noncovalent interaction energies from wavefunction theories for large molecules,” **Nat. Commun.** **16**, 9108 (2025).

<sup>122</sup>P. R. Nagy, L. Gyevi-Nagy, and M. Kállay, “Basis set truncation corrections for improved frozen natural orbital ccscd(t) energies,” **Mol. Phys.** **119**, e1963495 (2021).

<sup>123</sup>D. Cieślinski, A. M. Tucholska, and M. Modrzejewski, “Post-kohn–sham random-phase approximation and correction terms in the expectation-value coupled-cluster formulation,” **J. Chem. Theory Comput.** **19**, 6619–6631 (2023).

<sup>124</sup>F. Della Pia, A. Zen, D. Alfè, and A. Michaelides, “How accurate are simulations and experiments for the lattice energies of molecular crystals?” **Phys. Rev. Lett.** **133**, 046401 (2024).

<sup>125</sup>T. N. Mihm, T. Schäfer, S. K. Ramadugu, L. Weiler, A. Grüneis, and J. J. Shepherd, “A shortcut to the thermodynamic limit for quantum many-body calculations of metals,” **Nat. Comput. Sci.** **1**, 801–808 (2021).

<sup>126</sup>V. A. Neufeld, H.-Z. Ye, and T. C. Berkelbach, “Ground-state properties of metallic solids from ab initio coupled-cluster theory,” **J. Phys. Chem. Lett.** **13**, 7497–7503 (2022).

<sup>127</sup>J. P. Carbone, A. Irmller, A. Gallo, T. Schäfer, W. Z. Van Benschoten, J. J. Shepherd, and A. Grüneis, “Co adsorption on pt(111) studied by periodic coupled cluster theory,” **Faraday Discuss.** **254**, 586–597 (2024).

<sup>128</sup>T. Schäfer, “Ground states for metals from converged coupled cluster calculations,” **J. Phys. Chem. Lett.** **16**, 17–23 (2025).

<sup>129</sup>G. P. Chen, M. M. Agee, and F. Furche, “Performance and scope of perturbative corrections to random-phase approximation energies,” **J. Chem. Theory Comput.** **14**, 5701–5714 (2018).

<sup>130</sup>A. Heßelmann, “Third-order corrections to random-phase approximation correlation energies,” *J. Chem. Phys.* **134**, 204107 (2011).

# Supporting Information for Random phase approximation-based local natural orbital coupled cluster theory

Ruiheng Song,<sup>1</sup> Xiliang Gong,<sup>1</sup> Aamy Bakry,<sup>1</sup> and Hong-Zhou Ye<sup>1,2, a)</sup>

<sup>1)</sup>*Department of Chemistry and Biochemistry, University of Maryland, College Park, Maryland, 20742*

<sup>2)</sup>*Institute for Physical Science and Technology, University of Maryland, College Park, Maryland, 20742*

(Dated: 5 January 2026)

---

<sup>a)</sup>Electronic mail: [hzye@umd.edu](mailto:hzye@umd.edu)

## I. BASIS SETS AND GEOMETRIES

The solid-optimized cc-pVTZ basis sets for Cu, as well as the fitting basis sets for Cu and Li used in this work, are available in the following GitHub repository:

[github.com/hongzhouye/supporting\\_data/tree/main/2026/RPALNOCC](https://github.com/hongzhouye/supporting_data/tree/main/2026/RPALNOCC)

The same repository also contains the structure files for the C2C2PD molecular dimer and the anthracene molecular crystal, including all geometries required for counterpoise corrections.

## II. SUPPLEMENTARY DATA

TABLE S1. Lattice energy of the anthracene molecular crystal calculated by HF, MP2, and RPA using  $1 \times 1 \times 1$  and  $2 \times 2 \times 2$   $k$ -point meshes and the cc-pVTZ basis sets. The thermodynamic limit (TDL) results are obtained by linearly extrapolating the two finite  $k$ -mesh results with  $N_k^{-1}$  to  $N_k = \infty$ .

$N_k$	HF	MP2		RPA	
		Correlation	Total	Correlation	Total
		—	—	—	—
$1 \times 1 \times 1$	—75.4	—11.6	—86.9	—2.7	—78.0
$2 \times 2 \times 2$	+3.5	—46.2	—42.7	—25.5	—22.0
TDL	14.7	—51.1	—36.4	—28.8	—14.0

TABLE S2. Per-atom correlation energy calculated by different methods for BCC Li and FCC Cu using different basis sets and  $k$ -point meshes. The CCSD results for  $2 \times 2 \times 2$ /DZ and  $3 \times 3 \times 3$ /DZ are from canonical  $k$ -point CCSD, while all others are the best extrapolated values from LNO-CCSD as explained in the main text.

System	$N_k$	Basis set	MP2	RPA	RPA+SOSEX	CCSD
BCC Li	$3 \times 3 \times 3$	TZ	-0.0604	-0.0862	-0.0488	-0.0630
	$2 \times 2 \times 2$	DZ	-0.0344	-0.0478	-0.0276	-0.0388
BCC Li	$3 \times 3 \times 3$	DZ	-0.0463	-0.0535	-0.0325	-0.0434
	$4 \times 4 \times 4$	DZ	-0.0534	-0.0557	-0.0346	-0.0452
FCC Cu	$2 \times 2 \times 2$	TZ	-0.5583	-0.4823	-0.3789	-0.4690